Physisorption and desorption of H₂, HD and D₂ on amorphous solid water ice. Effect on mixing isotopologue on statistical population of adsorption sites†

Lionel Amiaud,‡*[a] Jean-Hugues Fillion,‡[b] François Dulieu,‡[c] Anouchah Momeni‡[a] and Jean-Louis Lemaire‡[ad]

We study the adsorption and desorption of three isotopologues of molecular hydrogen mixed on 10 ML of porous amorphous water ice (ASW) deposited at 10 K. Thermally programmed desorption (TPD) of H₂, D₂ and HD adsorbed at 10 K have been performed with different mixings. Various coverages of H₂, HD and D₂ have been explored and a model taking into account all species adsorbed on the surface is presented in detail. The model we propose allows to extract the parameters required to fully reproduce the desorption of H₂, HD and D₂ for various coverages and mixtures in the sub-monolayer regime. The model is based on a statistical description of the process in a grand-canonical ensemble where adsorbed molecules are described following a Fermi–Dirac distribution.

The desorption of molecular ices is important in a number of astrophysical environments including interstellar medium, cometary nuclei and the surface and atmospheres of planets. This transformation cannot be reduced to simple phase transitions of pure ices above their sublimation temperatures. There is additional complexity due to the structure of ices (amorphous, homogeneously mixed or layered) depending on their history and on the interplay with side processes that may be simultaneously triggered, like diffusion, photo-chemistry, radio-chemistry... In recent years, numerous laboratory studies have been performed on surfaces in order to mimic the molecular ices that are condensed or formed on cold dust grains particles (10 K) in dense molecular clouds. An overview of the current level of understanding of the adsorption and desorption of astrophysically relevant molecules on a variety of surfaces has been given by Burke and Brown.[1] The interaction of volatile species on

amorphous solid water (ASW) is of particular interest in the context of astrophysics, since water is the main component of molecular ices and because amorphous H₂O phase is believed to form in low temperature environments (<130 K).[2]

The ability of thick water ice samples to trap gas mixtures at very low temperature and release them well above their sublimation temperature has retained much attention in the 90's.[3–6] Later on, TPD (thermally programmed desorption) studies of volatiles adsorbed on the top or in the bulk of dense or porous ASW films have revealed the importance of the water-ice surface morphology to interpret the multiple desorption peaks observed.[7–12] Even if it is probable that astrophysical ices have a reduced porosity, after photoprocessing,[13] particles bombardment[14] and chemical processing,[15] porous ASW is believed to be a valuable analogue of interstellar ices. Typical desorption spectra of physisorbed molecules on ASW doesn't occur entirely in the low temperature domain (<70 K), as expected for weakly-bound species. These spectra are characterized by additional desorption features in the high temperature domain (140–170 K) corresponding to molecules trapped in the water ice during warming-up and then released in the gas phase by the so-called "volcano desorption" process (desorption associated to water ice crystallization) and "co-desorption" process (desorption concomitant to H₂O desorption itself). The fraction of molecules trapped within the ice and released at high temperature is linked to the diffusion of the molecule in the porous structure of ASW and to the continuous change of the water structure upon heating, as typically shown for CO.[9] Conversely, thermal heating of ice mixtures can induce diffusion of volatiles which can

a Institut des Sciences Moléculaires d'Orsay (ISMO), CNRS, University Paris-Sud, Université Paris-Saclay, F-91405 Orsay, France. E-mail: lionel.amiaud@u-psud.fr; Fax: +33 (0)1 69157671; Tel: +33 (0)1 69157684

b LERMA, Observatoire de Paris, PSL Research University, CNRS, Sorbonne Universités, UPMC, University Paris 06, F-75252, Paris, France

c LERMA, Observatoire de Paris, PSL Research University, CNRS, Sorbonnes Universités, UPMC University Paris 06, Université de Cergy-Pontoise, F-95000, Cergy-Pontoise, France

d LERMA, Observatoire de Paris, PSL Research University, CNRS, Sorbonnes Universités, UPMC Univ. Paris 06, France

† Electronic supplementary information (ESI) available: Demonstration of relations (7) used in the article. See DOI: 10.1039/c5cp03985a

‡ All author were member of LERMA and Université de Cergy Pontoise when experiments were carried out.

30148 | *Phys. Chem. Chem. Phys.*, 2015, **17**, 30148–30157

This journal is © the Owner Societies 2015

lead to the segregation of the ice components. For example, entrapment and segregation dynamics have been quantified and modeled for $CO_2 : H_2O$ and $CO : H_2O$ ice mixtures.[16–18]

Thermal desorption is governed according to the relative strength of the intermolecular forces between each component of the ices. Thus, the general description of binary ices requires the knowledge of their own binding energies in pure ice, in addition to the intermolecular binding energy between the two components. When these energies are very close to each other, it becomes difficult to analyze the combined thermal desorption curves and separate the desorption kinetics of each ice component. A first example can be found with water dominated ices, where very complex TPD spectra can be observed when molecule–water and water–water interaction energies are similar. This is typically observed for small organic species presenting hydrogen-bonds with water, such as binary layered $CH_3OH–H_2O$ and $C_2H_2OH–H_2O$ TPD curves that are very sensitive to the thickness of the underlying water and to the exposures used in the experiment.[19–21] Much complexity arises by the temperature-induced mixing between the two molecular layers. Also slight variation in the molecule-water interaction can lead to significant change in the thermal desorption behaviour, as shown by the comparison between isomers such as acetic and methyl formate, or ethanol and dimethyl-ether.[22,23] Another case of complex desorption is observed in the low temperature domain for small volatiles molecules. For example, the desorption of pure N_2 or pure CO ices occurs in the 25–30 K temperature range, since the binding energy between N_2 molecules and between CO molecules are very close (68 meV and 76 meV respectively). Consequently, the desorption kinetics of binary $CO–N_2$ ices (mixed or layered) is affected by the competition between the desorption of the two compounds.[24] The comparison between TPD curves of pure, mixed and layered ices demonstrate that thermal diffusion inducing both mixing and segregation mechanisms play important roles.[22,24,25] Similar complexity was found in $CO–O_2$ binary ices system.[26]

This article is a late follow-up of a previous paper[27] and will focus on the effect of isotopic mixing of absorbates on an amorphous solid water ice surface. It demonstrates clearly the role of competing mechanisms that occurs during the desorption process. In the present study, competition between the desorption of molecular hydrogen isotopologues (H_2, D_2 and HD) adsorbed on top of ASW is investigated in the 10–30 K temperature range. In this case, the binding energies of these molecules on ASW are extremely close to each other (a few meV).[27] Similarly to what has been observed in binary ices, such situation is expected to favor complex desorption spectra, when several isotopologues are mixed together on the water ice substrate. However several specificities of the system investigated here should be pointed out. At first, the present investigation is entirely conducted at hydrogen sub-monolayer coverage between 10 K and 30 K (multilayer of molecular hydrogen cannot be grown above 7 K[28]). In addition, water ice reorganization is very limited in the present temperature range, and can be completely avoided by a preliminary minor annealing that cancel further structural rearrangements of the substrate. By contrast to the examples given above,

this precludes diffusion of water molecules, which is one of the main processes leading to trapping and segregation, and the desorption is not driven by substrate modification. Consequently, the thermal desorption kinetics of molecular hydrogen is fully governed by surface processes, including surface diffusion and desorption.

In this context, the high heterogeneity of the ASW surface plays a fundamental role. Experiments on desorption processes of N_2 from ASW show that desorption is affected by the morphology of the ice and that TPD are characterized by a spreads over a relatively large temperature range (20–50 K).[29] The porosity of ASW tends to shift thermal desorption of volatiles to higher temperature with ASW film thickness.[28,30,31] In previous studies, we have already characterized the surface morphology of ASW through D_2 thermal desorption[32,33] and shown that D_2 physisorption energies are continuously distributed in the 30–70 meV energy range. This relatively wide range of binding energies added to the high mobility of molecular hydrogen in the whole 10–30 K temperature range has motivated the application of a simple model, in which the occupancy of the various binding sites available on the heterogeneous surface are described statistically, using a Fermi–Dirac law.[27,32,33] This model has been first applied to the description of the H_2 and D_2 desorption from ASW, in order to reproduce a surprising strong segregation phenomenon observed when both isotopes H_2 and D_2 were mixed on top of porous ASW sample. This effect, induced by the competition between H_2 and D_2 to fill the same binding sites, is governed by the spread of the binding energy distribution.[27]

We now present a more detailed and systematic experimental investigation of TPD spectra of molecular hydrogen isotopologues mixed at various coverages on ASW, and compare them to simulations based on our statistical model. In order to test the validity of the model, three isotopologues H_2, HD, D_2 interacting with porous ASW are considered. In addition to tertiary ice systems involving two isotopologues, the treatment is applied to quaternary ices, when the three isotopologues are simultaneously mixed on ASW. The article is organized as follows. Experimental set-up and details on experimental protocols are given in Section 1. Section 2 presents the experimental results for pure and mixed istolopologues successively. The model is described in Section 3. Finally, results are discussed in Section 4.

1 Experiments

In an ultrahigh vacuum chamber, with base pressure below 10^{-10} mbar, ASW films are grown on an oxygen-free high conductivity (OFHC) copper sample holder, cooled by a closed cycle He cryostat (ARS Displex DE-204S). The temperature is measured with a calibrated Silicon-diode sensor and a thermocouple (AuFe/Cromel K-type) and regulated by a Lakeshore 340 controller. It allows to set the temperature of the sample from 9 K to 350 K using a retro-control loop between temperature and power released by a heater cartridge clamped close to the sample holder. Temperature calibration has been achieved following Schlichting *et al.*[34] This allows an accuracy in the measured temperature better than 1 K. In the low temperature range,

This journal is © the Owner Societies 2015

Phys. Chem. Chem. Phys., 2015, **17**, 30148–30157 | **30149**

9 K to 35 K, this accuracy is stable within a 0.2 K range. This value is given by the maximum temperature shift observed in two identical experiments.

1.1 Water ice sample

The amorphous ice is made from deionised water (18 MΩ) purified initially and just before ice deposition by several freeze-thaw cycles under vacuum. The ice sample is grown by introducing water vapor in the chamber with a micro-capillary array doser. During this operation, the purity of the gas introduced in the chamber is controlled by monitoring residual pressure with a quadrupole Mass Spectrometer (QMS, HIDDEN 3F/PIC). The partial pressure is composed of H_2O and H_2 at more than 999/1000. The ice growth is controlled in two successive steps. The first step is the build-up of a thick ice film of 150 ML ($1 \text{ ML} = 10^{15} \text{ cm}^{-2}$) of compact ASW, with sample temperature stabilized at 120 K. During this operation, the doser is close to the surface to avoid chamber contamination by water. This first film is used to isolate the second film from the copper substrate. The second film is grown with the doser located far from the surface. The sample is exposed to a partial pressure of water close to 10^{-8} mbar whereas the substrate temperature is kept at 10 K. The exposition time is chosen to grow 10 ML. The water ice grown in this condition is amorphous and highly porous.[29] This ice is then annealed to 32 K which induces a slight modification (compaction) of the porous network. This first blank TPD experiment is performed to induce once for all any change that the sample may encounter when annealed to 32 K, like pores collapsing or few rearrangement in the disordered water molecule network. All TPD presented here were performed afterward on the same sample whose temperature never exceeded 30 K after the first annealing. The linear heating ramp used for TPD experiments is set from 10 K to 30 K at 10 K min^{-1}. The deviation error from the ideal linear heating is better than 0.1 K.

Once the ice film is prepared, the experimental protocol is the following: the ice sample is cooled down to 10 K and it is immediately exposed to a partial pressure (2×10^{-9} mbar) of a chosen isotopologue of molecular hydrogen (grade 4 purity). The amount of gas exposure is carefully controlled by monitoring partial pressure in the chamber with both the QMS and a Bayard-Alpert gauge. If more than one isotopologue is deposited, exposures are made sequentially, but results appear to be independent of the deposition order. After the exposure, molecular hydrogen desorption rates are measured with the QMS during the heating ramp. For H_2, the constant background signal has been subtracted. The integrated desorption signal, which is a measure of the amount of desorbed molecules from the sample, is proportional to the exposed doses below 4 ML. This linearity indicates a constant sticking coefficient until saturation at 4 ML exposition.[32,35,36] This value, larger than a monolayer, still stands in the sub-monolayer regime because of the large effective area of the highly porous ice. We have explored different values for the heating ramp (values from 0.016 K s^{-1} to 5 K s^{-1}), without observing any noticeable change on the TPD but the expected proportionality of the desorption

rate with the heating ramp. The determining parameter in these experiments is the initial dose. The doses of molecular hydrogen are expressed in term of ML, assuming perfect sticking efficiency for the three isotopologues. This assumption may not be valid for a non porous surface,[36,37] but is much more realistic on porous ASW (as it is the case here), for which multiple collisions within pores enhance the sticking. Values close to unity have indeed been reported for the sticking coefficient of D_2 on ASW.[28]

2 Results

2.1 Pure isotopologue

Fig. 1 shows TPD spectra for three pure isotopologues of molecular hydrogen H_2, HD and D_2, on 10 ML of ASW grown at 10 K, annealed at 32 K and held at 10 K during the hydrogen exposure. For each species, a set of TPD is represented, with different exposure dose lower than 4 ML which means for different initial submonolayer coverage. The multilayer of molecular hydrogen is expected to appear below 7 K, thus even the largest dose do not correspond to a multilayer coverage regime. The three spectra for each isotopologue represent a low dose, an intermediate dose and the maximum possible dose at 10 K without observing
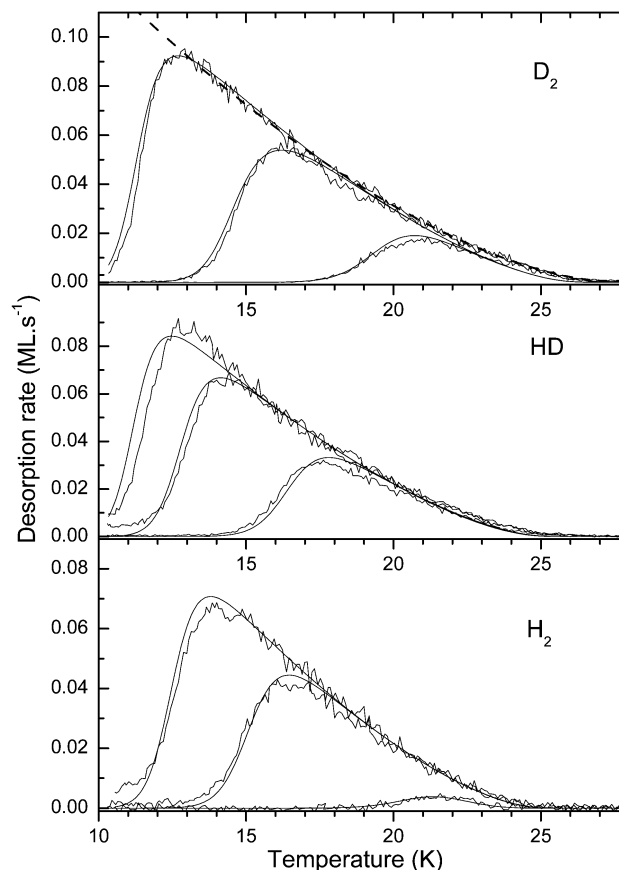

Fig. 1 Set of three TPD experiments for H_2, HD and D_2. Exposure doses in ML: 0.7, 1.4 and 2.6 for H_2; 1.0, 2.4 and 3.3 for HD; 0.5, 2.0 and 4.0 for D_2. Smooth lines are model adjustment (see Section 3). Dashed line on top panel shows a $(T_0 - T)^{1.6}$ law for the trailing edge.

30150 | Phys. Chem. Chem. Phys., 2015, 17, 30148–30157

This journal is © the Owner Societies 2015

immediate desorption. Indeed, increasing the dose above the highest one would lead to a desorption of the adsorbate before the TPD starts, and the proportionality between deposited dose and desorbed quantity would be lost.

We observe on Fig. 1 that, from one isotope to the other, the TPD are very similar, with two noticeable properties. Firstly, the desorption of large dose occurs over a broad range of temperature, typically from 10 K to 25 K. It means that the range of adsorption energies related to physisorption of molecular hydrogen on ASM is wide, as already commented in Amiaud et al.[32] This is due to the strong heterogeneity of the amorphous porous surface of the water ice. Secondly, smaller doses start to desorb at higher temperatures, leading the TPD curves to share their trailing edges. This filling behaviour means that adsorbed molecules are mobile enough to fast diffuse toward the strongest adsorption site prior to desorption.[28,29,32,33,38] This behaviour also supports the model for desorption described in Section 3, in which the fast diffusion ensure an equilibration of the molecules over the available binding sites. Thus, the common trailing edge reflects the number of adsorption sites available, as a function of their desorption temperature for each isotopologue. The trailing edge shape follows roughly a power law variation with power of 1.6, (Fig. 1, D_2, dashed line). Several profiles have been checked (log-normal, Gaussian, and mixture of Gaussian and linear functions) but the power law gives the best fits with the advantage of three parameters only.

Although the global shape of the TPD curves is similar, a more detailed comparison between the desorption from equivalent doses of pure H_2, HD and D_2 reveals leading and trailing edges differences for the three isotopologues (Fig. 2). With respect to H_2, the curves for HD and D_2 are shifted by 1 K and 1.5 K toward higher temperatures respectively. It suggests that heavier isotopologues are slightly more bound to the surface.

Trapping potential of the physisorption well, mainly defined by the surface potential and the polarisability of the physisorbed molecule, can be considered constant with isotopic exchange. Thus, electrostatic forces are equivalent and the motion is driven by a square root function of the inverse of mass. Increasing the mass reduces the zero-point energy (ZPE) and thus increases the

binding energy resulting in a delayed desorption on the temperature scale. TPD curve of D_2 is shifted with respect to that of HD (and HD with respect to that of H_2) by typically 1 K/25 K = 4%, consistent with the fact that the difference for the ZPE energies is typically 4% of the mean adsorption energy. It should be noticed in addition that such a temperature shift can be attributed either to an adsorption energy increase or to a decrease of the desorption efficiency. The latter is related to the pre-exponential factor in the Polanyi–Wigner equation (see eqn (1) in Section 3). These pre-exponential factors are however extremely difficult to obtain with enough precision to be compared here. In conclusion, the shift in energy is mainly assigned to the ZPE, although a variation of the pre-exponential factor could in principle also contribute.

2.2 Mixed isotopologues experiments

The dependence of the adsorption energy with the isotopologue leads to an interesting behaviour when they are mixed on ASW surface and when their desorption is simultaneously measured (Fig. 3 and 4). Desorption curves of the three mixed isotopologues are different from the desorption curves of pure isotopologues individually recorded. Lighter species, H_2 and HD are shifted to lower temperatures, whereas D_2 desorption occurs more efficiently at higher temperatures. D_2 desorption is nevertheless still starting at low temperatures but with a gentle leading edge slope. Moreover, these differences depend on the mixture ratio. This is for example remarkable in third row of Fig. 4: a dose of H_2 (in blue), is gradually moved to lower temperatures when an increasing D_2 dose is co-adsorbed (in red). This is the proof that even though isotopologues are dosed sequentially, they diffuse, mix and rearrange on the surface before desorption. Before desorption starts, the adsorbed species have reached an equilibrium on the surface, where they have to share a fixed amount of common adsorption sites. As TPD curves are independent of the dosing sequences but only depend on the quantities adsorbed, this equilibrium should be rapidly achieved at 10 K. We point out that even small D_2 doses adsorbed at 10 K on large H_2 quantities
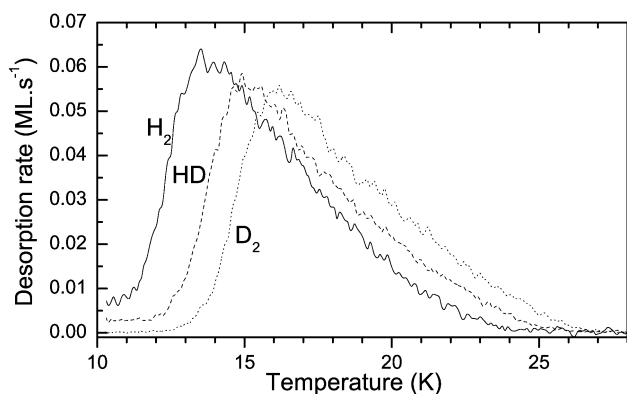

Fig. 2 Individual records of three TPD of pure H_2, HD and D_2 adsorbed at 10 K on 10 ML ASW grown at 10 K. Exposition doses are 2.2, 2.0 and 2.0 ML for H_2, HD and D_2 respectively.
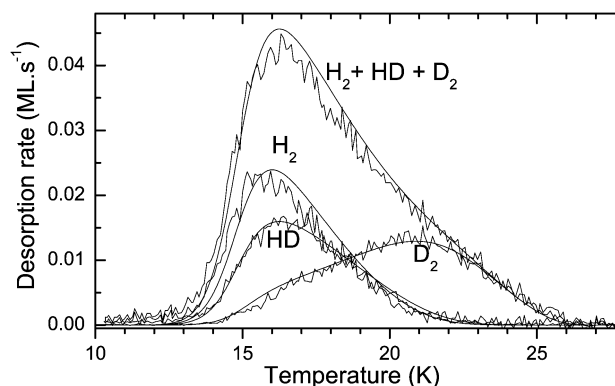

Fig. 3 TPD experiment for a mixed sub-monolayer adsorption of isotopologues: H_2 1.3 ML, HD 1.0 ML and D_2 0.7 ML. An artificial TPD for molecular hydrogen desorption regardless its isotope nature has been plotted summing up the three curves. Smooth lines: results of simulation, see Section 3.
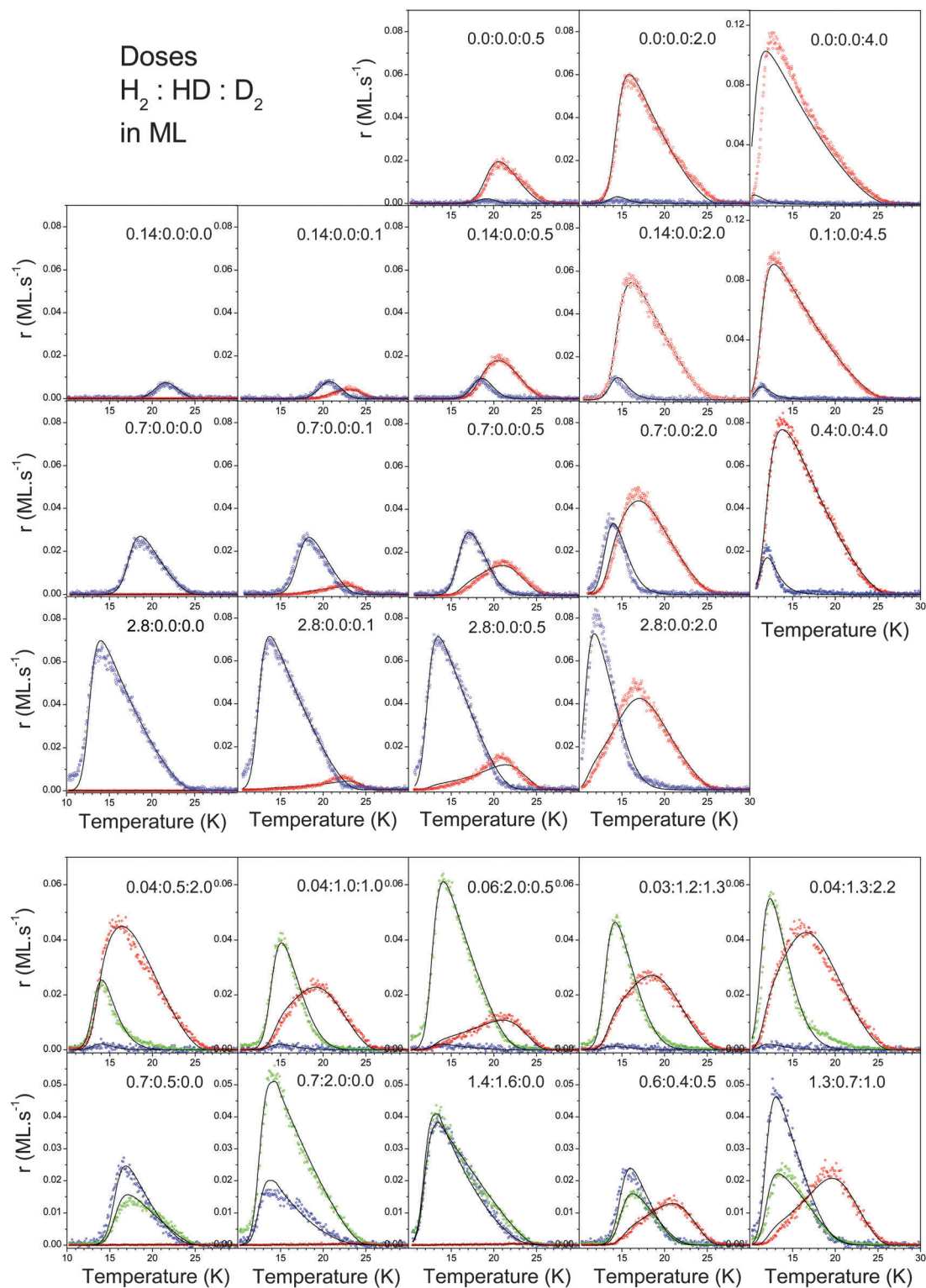
This journal is © the Owner Societies 2015

Phys. Chem. Chem. Phys., 2015, 17, 30148–30157 | 30151

Fig. 4   Experiments and simulated TPD for differents dose of mixed isotopes of molecular hydrogen adsorbed on 10 ML of ASW condensed at 10 K. H_2 blue circle, HD green circle and D_2 red circle. Initial coverage labeled as quantities H_2 : HD : D_2 expressed in ML. Solid curves show results from the model (see Section 3 for details).

are able to reach adsorption sites desorbing at 25 K. It gives an upper-limit for the diffusion barrier equal to the desorption barrier divided by 2.5. During TPD, molecules have then the ability to change from one adsorption site to another by thermal hopping at a rate faster than the desorption rate. They are consequently forced to desorb preferentially in a new set of

temperature range, especially at lower temperatures as compared to that from a pure sample. The origin of the shifts needs to be distinguished from that observed in TPD using thicker ice samples.[28,30,33] In these latter studies, the shifts are attributed to the variation of number of adsorption site available on the surface, resulting in a clear dependence with ice thickness and morphology. In the present study, the total number of adsorption site does not change from one experiment to the other performed with different mixtures. But during a TPD, the partition of the adsorption sites between the different isotopologues is varying depending on their respective amounts. To stress the role played by this dynamic occupancy of adsorption sites, we have plotted on Fig. 3 the sum of the three TPD curves. This fictive TPD is similar to a TPD of any molecular hydrogen isotopologue. From this point of view, blind to the isotopic nature of molecular hydrogen, the desorption follows the same desorption law than any single isotopologue. For the same reason, it explains why above 20 K, at which a majority of the 2 other isotopologues have left the sample (Fig. 3), the shape of the D_2 desorption curve recovers exactly that of a pure sample, independently of the distortion observed at lower temperatures. As thermal hopping that allows a molecule to explore available adsorption site is faster than desorption, we can reasonably state that desorption sites are permanently reallocated over the TPD experiment during the heating ramp. This suggests that thermal equilibrium is achieved for the adsorption site population all along the desorption. This fact supports again the main assumption of the model detailed it the next section.

The TPD experiments mixing the isotopologues have been repeated by varying the $H_2 : HD : D_2$ ratio (Fig. 4). The top panels show the behaviour of $H_2 : D_2$ mixtures for increasing D_2 coverages (from left to right) and increasing H_2 coverages (from top to bottom). Considering a column, one can follow the desorption behaviour of the species co-adsorbed on the surface. At any fixed D_2 coverage, D_2 desorption curves appear almost insensitive to the presence of H_2, and D_2 desorbs systematically at higher temperatures as compared to H_2. However, for H_2 dominating in the mixture (last row), one can note that D_2 desorption curves progressively deviate from their desorption behaviour in a single-component experiment, especially below 20 K where the two species D_2 and H_2 are simultaneously desorbing, leading to a D_2 desorption curve abnormally spreading towards lower temperatures. This behaviour reveals the importance of the relative composition and total coverage to control the desorption of one individual species in the temperature range where both species are expected to desorb. The bottom panel presents a series of results from tertiary samples with various relative ratio. Again, one can observe that D_2 desorption curves tend to be distorted in the lower temperature range, while at the same time H_2 and HD show a very similar kinetics. Also the high sensitivity of these desorption profiles to the initial relative concentration gives rise to relatively complex curves, that can be different from that obtained from a single-adsorbate system with the same total coverage. This sensitive behaviour makes any prediction difficult without a refined model describing the desorption kinetics.

3 Model of the desorption

Understanding the desorption during a TPD experiment means being able to explain the evolution of the desorption rate along the increase of the temperature. The desorption rate is commonly expressed by the Polanyi–Wigner equation:

$$r = -\frac{dN}{dt} = -A(N)N^n e^{-E(N)/kT} \quad (1)$$

where T is the temperature, N is the number of adsorbed molecules, k is the Boltzmann constant, $A(N)$, the efficiency factor, is the number of desorption attempt (s^{-1} molecules^{1-n}), and can vary with the coverage. n is the desorption order (here $n = 1$ for physisorption of molecular hydrogen on ASW in sub-monolayer regime), and $E(N)$ the coverage-dependent activation energy for the desorption.

Several methods are used to invert eqn (1), and obtain $E(N)$ and $A(N)$.[39–41] They must be used with care because errors in the determination of this two quantities can compensate each other.[40] The classical Arrhenius plot method is not well adapted in the case of physisorption of hydrogen on ASW as explored in Amiaud *et al.*[32] Pre-exponential factor obtained this way are uncertain. Tait and coworker (2005)[42] have shown that both determination of a constant pre-exponential factor and $A(N)$ can be done with a least square method in the case of N_2 desorption from ASW. It is not conclusive in our experiments, and cannot predict the observed isotopic effect.

A model for the desorption of single isotopologue experiment have already been presented in Amiaud *et al.*[32] In a nut shell, it is built on few assumptions strengthened by simple thermodynamic arguments. Thermal hopping at 10 K is efficient and physisorbed molecules are highly mobile on the surface, as suggested by the TPD profiles. The mobility of adsorbed molecules allows the system to explore a number of configurations large enough for the ergodic hypothesis to be assumed. The thermal equilibrium on the surface is achieved all along the desorption process so that adsorption site filling follows a Fermi–Dirac statistical distribution. This is the appropriated statistic for a grand canonic system where adsorption sites can be filled by only one molecule. Moreover, experiments are performed in UHV chamber in which there is no sensible increase of partial pressure of molecular hydrogen during TPD experiment. The molecular hydrogen returning from the gas phase to surface during TPD experiment can be ignored.

The number of adsorption sites for is a set g_{H_2} given as a function of the energy by:

$$g_{H_2}(E) = \begin{cases} a(E_t - E)^{1.6} & \text{for} \quad E < E_t \\ 0 & \text{for} \quad E \geq E_t \end{cases} \quad (2)$$

E_t is a threshold energy above which $g_{H_2}(E)$ is zero. The 1.6 power law, determined in Amiaud *et al.*[32] as the best agreement between experiment and modeling on a 10 ML porous ASW ice, reflect also the shape of the trailing edge in TPD curve (see Fig. 1). a is a scale parameter, identical for the three species, that can be adjusted. HD and D_2 share the same sites distribution

shifted by a constant ZPE difference. In the following, we treat the three isotopologues with same equations, designing by letter X the concerned isotopologue, and Y and Z the two other. The expression for the site distribution of an isotopologue X is then:

$$g_X(E) = g_{H_2}(E - \Delta E_X) \qquad (3)$$

with ΔE_X the energy shift due to the ZPE, set at $\Delta E_{H_2} = 0$ for H_2, the reference.

The population $P_X(E)$ of an isotopologue X is then given as a Fermi–Dirac distribution over the set of available adsorption sites for X:

$$P_X(E) = \{g_X(E) - O_Y(E) - O_Z\} \times \mathrm{FD}(E, \mu_X, T) \qquad (4)$$

where $\mathrm{FD}(E, \mu_X, T)$ is the Fermi–Dirac distribution, O_Y and O_Z are the occupancy of adsorption sites by other isotopes.

$$\mathrm{FD}(E, \mu_X, T) = \left(1 + e^{-(E - \mu_X)/k_B T}\right)^{-1} \qquad (5)$$

O_Y and O_Z can be simply deduced from population P_Y and P_Z, considering the ZPE shift:

$$O_Y(E) = P_Y(E + (\Delta E_Y - \Delta E_X))$$
$$O_Z(E) = P_Z(E + (\Delta E_Z - \Delta E_X)) \qquad (6)$$

By combining the three eqn (4) obtained by permuting X, Y and Z and eqn (3), we deduce the general expression $P_X(E)$ of an isotopologue X mixed with Y and Z in a common set g of adsorption sites, with ZPE shift. (The demonstration in the general case of a finite number n of species, sharing a common set of adsorption site with an energy shift, is available in ESI†.)

$$P_X(E) = g_X(E) \times \left\{ 1 + e^{-(E - \mu_X)/k_B T} \right.$$
$$+ e^{-(\Delta E_X - \Delta E_Y - (\mu_X - \mu_Y))/k_B T}$$
$$\left. + e^{-(\Delta E_X - \Delta E_Z - (\mu_X - \mu_Z))/k_B T} \right\}^{-1} \qquad (7)$$

In this expression, μ_X is the chemical potential, the most probable adsorption energy for any new molecule X added in the system. The lower μ_X, the more X molecules populate the $g(E)$ distribution. In addition, unless temperature were 0 K, molecules can be found in adsorption site of weak energy even if adsorption sites of stronger energy are not fully occupied. This formulation shows also the rule of the competition for adsorption sites between the isotopologues. A molecule X is found less probably at a given energy E if the corresponding adsorption energy for another isotopologue Y is much higher, i.e. $\Delta E_X < \Delta E_Y$; unless the total number of X molecules on the surface is high, i.e. $\mu_X \ll \mu_Y$. Populations can be calculated for a given temperature and given total adsorbed quantities N_{Xads}, N_{Yads} and N_{Zads} by finding the three μ that verify the three closing relations:

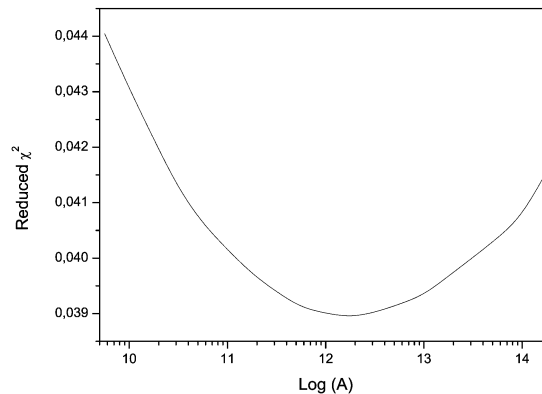$$N_{Xads} = \int P_X(E) \mathrm{d}E \qquad (8)$$

Fig. 5 Agreement between experiment and model expressed as reduced χ^2 for different fixed A parameters. All data presented Fig. 1 and 4 are taken in account.

Evolution of adsorbed quantities are deduced from the desorption rates r_X, given by eqn (1) integrated over E.

$$r_X = -\frac{\mathrm{d}N_{ads}}{\mathrm{d}t} = \int P_X(E) A e^{-E/k_B T} \mathrm{d}E \qquad (9)$$

The efficiency parameter A is taken constant, independent of the energy of adsorption site. This is a strong assumption as this parameter is known to vary with coverage[40,43,44] in the range 10^{10}–10^{13} s^{-1}. Values from 5×10^9 to 2×10^{14} s^{-1} were explored. By using a χ^2 criteria for fitting quality, the best results are obtained for A close to 1.8×10^{12} s^{-1} (Fig. 5). This value is not far from the 1×10^{13} s^{-1} taken in Amiaud et al.[32] and is comparable to result of theory.[32,45] A is expected to vary with adsorption energy and mass of the desorbing particle, depending on the depth of the physisorption well and the ZPE of the adsorbate in this well. If we consider also that, in term of desorption description, a small change in A value can be counterbalanced by a small change in E in eqn (1), then we can for simplicity reasons take a common value for H_2, D_2 and HD with $A = 1.8 \times 10^{12}$ s^{-1}.

The numerical computation of the desorption rates with temperature is done step-by-step. The initial coverage is calculated by summation of the measured desorption rate from 10 to 30 K. In principle, this quantity should be corrected by the detection efficiency of the mass spectrometer to reach absolute quantities. But practically, desorption rates calculated from this initial coverage can be directly compared to the desorption signal measured. All along the step-by-step simulation, populations over adsorption sites are calculated finding the μ_{H_2}, μ_{HD} and μ_{D_2} that verify eqn (8). Desorption rates are obtained from eqn (9) every seconds, i.e. every 0.17 K, and N_{Xads} are consequently updated. A fitting procedure has been applied over the set of 36 experiments (shown on Fig. 2 and 4) on 10 ML porous ASW annealed to 32 K, in order to adjust E_t, ΔE_{HD}, ΔE_{DD}, the scale factor a and the efficiency factor A. Only this five parameters are adjusted. Our model allows to reproduce the differences observed for H_2, HD and D_2 on the 36 experiments with various initial coverages of H_2, D_2 and HD, including pure isotope experiments. The full set of mixed experiments and

Table 1 Values used for TPD modeling on 10 ML of ASW

	Value	Unit
Adsorption site energy distrib.		
g	*cf.* eqn (2)	ML meV^{-1}
a	4.70×10^{-4}	ML meV$^{-2.6}$
E_t	67.5	meV
Shift between isotop. distrib.	*cf.* eqn (3)	
ΔE_{H_2}	0	meV
ΔE_{HD}	0.40	meV
ΔE_{D_2}	3.15	meV
Desorption efficiency A	1.8×10^{12}	s^{-1}

fitting results are shown Fig. 4. The parameter space is explored following a Newton's method, except for A. Table 1 summarizes the parameters used for the all TPD calculated.

4 Discussion

4.1 Molecular hydrogen adsorption energies

The good results of our TPD inversions procedure validates the assumption of a single adsorption energy distributions for the different isotopologues of H_2 but solely shifted. H_2 adsorption energies range from ≈ 30 to 67.5 meV, and HD and D_2 are more bounded. These differences are attributed to differences in ZPE in the physisorption well. A tentative estimation can be made, considering a harmonic physisorption potential. Considering a typical spatial extension of the well $\ell = 3 \times 10^{-10}$ m, the square root of typical surface density (10^{15} cm^{-2}), and a potential depth De ≈ 30–60 meV, the associated frequency is estimated to be $\nu_0 \propto \sqrt{\text{De}/m}\big/2\pi$, *i.e.* $\nu_0 \propto 10^{12}$ s^{-1}. This is consistent with A derived from our experiments, believed to be closed to the vibrational frequency of molecule in its physisorption well. Considering $\nu_0 = 10^{12}$ s^{-1}, in the harmonic approximation, the ZPE for H_2 (resp. HD and D_2) is $h\nu_0/2 = 1.77$ meV (1.45 and 1.25 meV). Table 1 shows differences between ZPE values that are of the order of magnitude of this estimation, but the shift in energy between H_2 and HD of 0.40 meV is small compared to that between H_2 and D_2 of 3.15 meV. Indeed, we have already noticed that in the TPD spectra of mixed species, H_2 and HD behave similarly whereas D_2 show distinct TPD curves. This behaviour is at first sight surprising in the harmonic approximation above. However, one should not forget to take into account the rotational state of the almost freely rotating molecules, since these states do not have the same adsorption energies. In this experiment, the molecules are condensed from a room temperature gas sample on the 10 K water surface. HD molecules are relaxing promptly into the $J = 0$ ground state. In the case of H_2, after deposition at 10 K, the population is frozen on the lowest states $J = 0$ (*para*-state) and $J = 1$ (*ortho*-state) with an *ortho/para* ratio of 3. For D_2, the lowest states are $J = 0$ (*ortho*-state) and $J = 1$ (*para*-state) with a *ortho/para* ratio of 2. Full relaxation into the rotational ground state requires nuclear spin conversion, occurring on ASW at long timescales in the absence of paramagnetic species.[46] Such conversion is not expected on the

timescales of few minutes used in these TPD experiments. It has been shown that hydrogen molecules in the non-isotropic $J = 1$ rotational states are slightly more bound to the surface that hydrogen molecules in their isotropic ground state.[47–50] In the absence of nuclear spin relaxation, one can consider that most H_2 molecules lies in their H_2 ($J = 1$) and are more strongly bound to the surface as compared to H_2 ($J = 0$). In parallel, HD ($J = 0$) are also more strongly bound to the surface due to ZPE by a same order of magnitude. In the case of HD, no spin relaxation applies and most of the population is expected in the $J = 0$ rotational state. This most probably explain why H_2 and HD have apparently similar binding energies in this experiment, and consequently similar behaviour. Since the shape of the desorption curves of mixtures appears to be very sensitive the binding energies, it would be very interesting to repeat such experiments using pure *ortho*- and *para*-H_2 (or D_2) separately to confirm this statement.

4.2 Desorption of ices mixtures

The present model reproduces very satisfactorily the TPD experiments, as shown in Fig. 4. This strengthens the fact that the high diffusion hypothesis is valid in the case of molecular hydrogen physisorbed on ASW. In the present context, the determination of the diffusion energies, as suggested by recent diffusion–desorption rate equation model[51] is not necessary. A limited number of parameters is sufficient to reproduce the series of desorption experiments at various doses and isotopic composition. In addition, it should be pointed out that this approach address correctly the desorption of tertiary mixtures desorbing simultaneously. In particular, the asymmetric behaviour between H_2 and HD on the one hand, and D_2 on the other hand, is well reproduced by the set of binding energies deduced from the experiment. This asymmetric behaviour have important consequences in the context of gas–ice interaction in the interstellar medium. The isotopic ratios resulting from adsorption–desorption of molecular hydrogen on ASW in this context has already been explored from an astrophysical point of view by Kristensen *et al.*[52]

5 Conclusions

In summary, we have characterized the desorption kinetics of molecular hydrogen on ASW between 10 and 30 K. We have explored the desorption behaviour of H_2, HD and D_2 on ASW studying their dynamics either separately, or mixed together at submonolayer coverage onto porous ASW. All the samples do show different behaviours during TPD experiment. The desorption of pure molecular hydrogen (single-component) has been analyzed using a simple Fermi–Dirac distribution law over a set of binding sites characterized by two parameters. The model applies in the context of high diffusion limit, as suggested by the common trailing edges of the TPD curves obtained from different surface coverage. The model consider a first order desorption kinetics to reproduce the experiment, using a standard efficiency factor for desorption and one distribution of binding energies that is shifted to higher energies for HD and D_2 as compared to H_2. We suggest

This journal is © the Owner Societies 2015

Phys. Chem. Chem. Phys., 2015, **17**, 30148–30157 | **30155**

that the shifts obtained by fitting the experimental data are mostly originating from the zero point energies, but that the population of H_2 into the first rotational excited state should also be taken account in addition to that of the ground state. The same model is applied to reproduce very satisfactorily the desorption of mixtures (multi-components), including especially the most challenging desorption from tertiary samples (H_2, HD and D_2). TPD curves obtained from the variety of ices mixtures explored in the present study depend on exact relative isotopic composition and coverage. The TPD curves of one isotopologue is governed by the competition with other species that desorb in the same temperature range. The model simulates correctly this competition, and indicates that due to continuous re-distribution of the population onto the same set of adsorption sites, lighter species (H_2 and HD) are forced to desorb at the lowest temperatures due to the presence of D_2. The present study highlights a very sensitive desorption mechanism correlated to the binding energies. It would be interesting to explore other weakly bound species in the sub-monolayer regime to investigate the ability of this model to describe other case of segregation.

References

1 D. J. Burke and W. A. Brown, *Phys. Chem. Chem. Phys.*, 2010, **12**, 5947–5969.

2 P. Ehrenfreund, H. J. Fraser, J. Blum, J. H. E. Cartwright, J. M. Garca-Ruiz, E. Hadamcik, A. C. Levasseur-Regourd, S. Price, F. Prodi and A. Sarkissian, *Planet. Space Sci.*, 2003, **51**, 473–494.

3 A. Bar-Nun, I. Kleinfeld and E. Kochavi, *Phys. Rev. B: Condens. Matter Mater. Phys.*, 1988, **38**, 7749–7754.

4 R. Hudson and B. Donn, *Icarus*, 1991, **94**, 326–332.

5 S. A. Sandford and L. J. Allamandola, *Icarus*, 1990, **87**, 188–192.

6 G. Notesco and A. Bar-Nun, *Icarus*, 1997, **126**, 336–341.

7 P. Ayotte, R. S. Smith, K. P. Stevenson, Z. Dohnálek, G. A. Kimmel and B. D. Kay, *J. Geophys. Res.*, 2001, **106**, 33387–33392.

8 N. Horimoto, H. S. Kato and M. Kawai, *J. Chem. Phys.*, 2002, **116**, 4375–4378.

9 M. P. Collings, J. W. Dever, H. J. Fraser and M. R. S. McCoustra, *Astrophys. Space Sci.*, 2003, **285**, 633–659.

10 M. P. Collings, J. W. Dever, H. J. Fraser, M. R. S. McCoustra and D. A. Williams, *Astrophys. J.*, 2003, **583**, 1058.

11 M. P. Collings, M. A. Anderson, R. Chen, J. W. Dever, S. Viti, D. A. Williams and M. R. S. McCoustra, *Mon. Not. R. Astron. Soc.: Lett.*, 2004, **354**, 1133–1140.

12 S. Viti, M. P. Collings, J. W. Dever, M. R. S. McCoustra and D. A. Williams, *Mon. Not. R. Astron. Soc.: Lett.*, 2004, **354**, 1141–1145.

13 M. E. Palumbo, *Astron. Astrophys.*, 2006, **453**, 903–909.

14 U. Raut, M. Famá, M. J. Loeffler and R. A. Baragiola, *Astrophys. J.*, 2008, **687**, 1070–1074.

15 M. Accolla, E. Congiu, F. Dulieu, G. Manico, H. Chaabouni, E. Matar, H. Mokrane, J. L. Lemaire and V. Pirronello, *Phys. Chem. Chem. Phys.*, 2011, **13**, 8037–8045.

16 R. Hodyss, P. V. Johnson, G. E. Orzechowska, J. D. Goguen and I. Kanik, *Icarus*, 2008, **194**, 836–842.

17 K. I. Öberg, E. C. Fayolle, H. M. Cuppen, E. F. van Dishoeck and H. Linnartz, *Astron. Astrophys.*, 2009, **505**, 183–194.

18 E. C. Fayolle, K. I. Öberg, H. M. Cuppen, R. Visser and H. Linnartz, *Astron. Astrophys.*, 2011, **529**, A74.

19 D. J. Burke, A. J. Wolff, J. L. Edridge and W. A. Brown, *J. Chem. Phys.*, 2008, **128**, 104702.

20 D. J. Burke, A. J. Wolff, J. L. Edridge and W. A. Brown, *Phys. Chem. Chem. Phys.*, 2008, **10**, 4956–4967.

21 A. J. Wolff, C. Carlstedt and W. A. Brown, *J. Phys. Chem. C*, 2007, **111**, 5990–5999.

22 M. Bertin, C. Romanzin, X. Michaut, P. Jeseck and J.-H. Fillion, *J. Phys. Chem. C*, 2011, **115**, 12920–12928.

23 M. Lattelais, M. Bertin, H. Mokrane, C. Romanzin, X. Michaut, P. Jeseck, J.-H. Fillion, H. Chaabouni, E. Congiu, F. Dulieu, S. Baouche, J.-L. Lemaire, F. Pauzat, J. Pilmé, C. Minot and Y. Ellinger, *Astron. Astrophys.*, 2011, **532**, A12.

24 S. E. Bisschop, H. J. Fraser, K. I. Öberg, E. F. van Dishoeck and S. Schlemmer, *Astron. Astrophys.*, 2006, **449**, 1297–1309.

25 K. I. Öberg, F. van Broekhuizen, H. J. Fraser, S. E. Bisschop, E. F. van Dishoeck and S. Schlemmer, *Astrophys. J., Lett.*, 2005, **621**, L33–L36.

26 K. Acharyya, G. W. Fuchs, H. J. Fraser, E. F. van Dishoeck and H. Linnartz, *Astron. Astrophys.*, 2007, **466**, 1005–1012.

27 F. Dulieu, L. Amiaud, S. Baouche, A. Momeni, J. H. Fillion and J. L. Lemaire, *Chem. Phys. Lett.*, 2005, **404**, 187–191.

28 L. Hornekaer, A. Baurichter, V. V. Petrunin, A. C. Luntz, B. D. Kay and A. Al-Halabi, *J. Chem. Phys.*, 2005, **122**, 124701.

29 G. A. Kimmel, K. P. Stevenson, Z. Dohnalek, R. S. Smith and B. D. Kay, *J. Chem. Phys.*, 2001, **114**, 5284–5294.

30 T. Zubkov, R. S. Smith, T. R. Engstrom and B. D. Kay, *J. Chem. Phys.*, 2007, **127**, 184707.

31 T. Zubkov, R. S. Smith, T. R. Engstrom and B. D. Kay, *J. Chem. Phys.*, 2007, **127**, 184708.

32 L. Amiaud, J. H. Fillion, S. Baouche, F. Dulieu, A. Momeni and J. L. Lemaire, *J. Chem. Phys.*, 2006, **124**, 094702.

33 J.-H. Fillion, L. Amiaud, E. Congiu, F. Dulieu, A. Momeni and J.-L. Lemaire, *Phys. Chem. Chem. Phys.*, 2009, **11**, 4396–4402.

34 H. Schlichting and D. Menzel, *Rev. Sci. Instrum.*, 1993, **64**, 2013–2022.

35 L. Amiaud, F. Dulieu, J.-H. Fillion, A. Momeni and J. L. Lemaire, *J. Chem. Phys.*, 2007, **127**, 144709.

36 E. Matar, H. Bergeron, F. Dulieu, H. Chaabouni, M. Accolla and J. L. Lemaire, *J. Chem. Phys.*, 2010, **133**, 104507.

37 H. Chaabouni, H. Bergeron, S. Baouche, F. Dulieu, E. Matar, E. Congiu, L. Gavilan and J. L. Lemaire, *Astron. Astrophys.*, 2012, **538**, A128.

38 E. Matar, E. Congiu, F. Dulieu, A. Momeni and J. L. Lemaire, *Astron. Astrophys.*, 2008, **492**, L17–L20.

39 A. M. de Jong and J. W. Niemantsverdriet, *Surf. Sci.*, 1990, **233**, 355–365.

40 W. Rudzinski, T. Borowiecki, T. Panczyk and A. Dominko, *Adv. Colloid Interface Sci.*, 2000, **84**, 1–26.

41 P. J. Barrie, *Phys. Chem. Chem. Phys.*, 2008, **10**, 1688–1696.

42 S. L. Tait, Z. Dohnalek, C. T. Campbell and B. D. Kay, *J. Chem. Phys.*, 2005, **122**, 164707.

43 E. Seebauer, A. Kong and L. Schmidt, *Surf. Sci.*, 1988, **193**, 417–436.

44 V. Zhdanov, *Surf. Sci. Rep.*, 1991, **12**, 185–242.

45 H. G. Hixson, M. J. Wojcik, M. S. Devlin, J. P. Devlin and V. Buch, *J. Chem. Phys.*, 1992, **97**, 753–767.

46 M. Chehrouri, J.-H. Fillion, H. Chaabouni, H. Mokrane, E. Congiu, F. Dulieu, E. Matar, X. Michaut and J. L. Lemaire, *Phys. Chem. Chem. Phys.*, 2011, **13**, 2172–2178.

47 V. Buch and J. P. Devlin, *J. Chem. Phys.*, 1993, **98**, 4195–4206.

48 L. Amiaud, A. Momeni, F. Dulieu, J. Fillion, E. Matar and J.-L. Lemaire, *Phys. Rev. Lett.*, 2008, **100**, 056101.

49 L. Gavilan, G. Vidali, J. L. Lemaire, M. Chehrouri, F. Dulieu, J.-H. Fillion, E. Congiu and H. Chaabouni, *Astrophys. J.*, 2012, **760**, 35.

50 K. Fukutani and T. Sugimoto, *Prog. Surf. Sci.*, 2013, **88**, 279–348.

51 J. He and G. Vidali, *Faraday Discuss.*, 2014, **168**, 517–532.

52 L. E. Kristensen, L. Amiaud, J.-H. Fillion, F. Dulieu and J.-L. Lemaire, *Astron. Astrophys.*, 2011, **527**, A44.